Inorg. Chem. **2008**, *47*, 3515−3520

Solution Dynamics and Gas-Phase Chemistry of $Pd_2@Sn_{18}^{4-}$

F. Sanem Kocak, Peter Zavalij, Yiu-Fai Lam, and Bryan W. Eichhorn*

Department of Chemistry and Biochemistry, University of Maryland, College Park, Maryland 20742

Received August 29, 2007

Sn_9^{4-} reacts with $Pd(PPh_3)_4$ in ethylenediamine/toluene solvent mixtures in the presence of 2,2,2-cryptand to give the $Pd_2@Sn_{18}^{4-}$ cluster as the $K(2,2,2,\text{-crypt})^+$ salt. The cluster is isostructural with $Pd_2@Ge_{18}^{4-}$ and has a nuclearity different from that of the Pt and Ni analogues, $Ni_2@Sn_{17}^{4-}$ and $Pt_2@Sn_{17}^{4-}$. The $Pd_2@Sn_{18}^{4-}$ ion has a deltahedral capsulelike structure with 40 cluster bonding electrons and is the largest free-standing polystannide characterized to date. Like $Pt_2@Sn_{17}^{4-}$, the $Pd_2@Sn_{18}^{4-}$ complex is highly dynamic in solution, showing a single ^{119}Sn NMR resonance indicative of an intramolecular liquidlike dynamic exchange. LDI-MS studies of the crystalline sample show extensive fragmentation and the formation of five gas-phase cluster series: Sn_x^- ($1 < x < 12$), $PdSn_{x-1}^-$ ($4 < x < 18$), $Pd_2Sn_{x-2}^-$ ($6 < x < 21$), $Pd_3Sn_{x-3}^-$ ($8 < x < 21$), and $Pd_4Sn_{x-4}^-$ ($13 < x < 21$). The most abundant ion in the gas phase is the $PdSn_{10}^-$ cluster, which presumably has an Sn_{10} bicapped-square-antiprismatic structure with an endohedral Pd (e.g., $Ni@Pb_{10}^{2-}$).

Introduction

Interest in highly symmetrical clusters derived from Zintl ions resides in their novel solid-state structures,[1,2] unusual electronic structures,[3–5] gas-phase chemistry,[6,7] solution dynamics,[8–10] and their similarities to the fullerenes[2] and icosahedral aluminates.[11,12] In addition, the ability to aggregate and polymerize these ions in a controlled fashion makes them ideal candidates for use in cluster assembled materials.[12–14] Recent efforts have focused on the Ge_{12}, Sn_{12}, and Pb_{12} icosahedra,[7,15–18] near icosahedra,[15,19,20] and fused icosahedra[8,10,21–23] containing endohedral transition metals.[2] The germanium compounds are largely derived from Ge_9^{4-} subunits and include $Ni_3@Ge_{18}^{4-}$,[23] $[Ni@Ge_9NiL]^{2-}$, where $L = PPh_3$, CO,[21,24,25] and $Pd_2@Ge_{18}^{4-}$.[22] The chemistry of Pb_9^{4-} is quite different and is characterized by facile fragmentation/disproportionation reactions to give 10- and 12-atom clusters such as $Ni@Pb_{10}^{2-}$ and $Pt@Pb_{12}^{2-}$.[15,16,20]

* To whom correspondence should be addressed. E-mail: eicchorn@umd.edu.

(1) Sevov, S. C.; Goicoechea, J. M. *Organometallics* **2006**, *25*, 5678–5692.
(2) Fassler, T. F.; Hoffmann, S. D. *Angew. Chem., Int. Ed.* **2004**, *43*, 6242–6247.
(3) King, R. B.; Heine, T.; Corminboeuf, C.; Schleyer, P. v. R. *J. Am. Chem. Soc.* **2004**, *126*, 430–431.
(4) Chen, Z. F.; Neukermans, S.; Wang, X.; Janssens, E.; Zhou, Z.; Silverans, R. E.; King, R. B.; Schleyer, P. v. R.; Lievens, P. *J. Am. Chem. Soc.* **2006**, *128*, 12829–12834.
(5) Boldyrev, A. I.; Wang, L. S. *Chem. Rev.* **2005**, *105*, 3716–3757.
(6) Waters, T.; Wang, X. B.; Wang, L. S. *Coord. Chem. Rev.* **2007**, *251*, 474–491.
(7) Cui, L. F.; Huang, X.; Wang, L. M.; Li, J.; Wang, L. S. *Angew. Chem., Int. Ed.* **2007**, *46*, 742–745.
(8) Esenturk, E. N.; Fettinger, J. C.; Eichhorn, B. W. *J. Am. Chem. Soc.* **2006**, *128*, 12–13.
(9) Kesanli, B.; Mattamana, S. P.; Danis, J.; Eichhorn, B. *Inorg. Chim. Acta* **2005**, *358*, 3145–3151.
(10) Kesanli, B.; Halsig, J. E.; Zavalij, P.; Fettinger, J. C.; Lam, Y. F.; Eichhorn, B. W. *J. Am. Chem. Soc.* **2007**, *129*, 4567–4574.
(11) Li, X.; Grubisic, A.; Stokes, S. T.; Cordes, J.; Gantefor, G. F.; Bowen, K. H.; Kiran, B.; Willis, M.; Jena, P.; Burgert, R.; Schnockel, H. *Science* **2007**, *315*, 356–358.
(12) Zheng, W. J.; Thomas, O. C.; Lippa, T. P.; Xu, S. J.; Bowen, K. H. *J. Chem. Phys.* **2006**, 124.
(13) Riley, A. E.; Tolbert, S. H. *Res. Chem. Int.* **2007**, *33*, 111–124.
(14) Sun, D.; Riley, A. E.; Cadby, A. J.; Richman, E. K.; Korlann, S. D.; Tolbert, S. H. *Nature* **2006**, *441*, 1126–1130.
(15) Esenturk, E. N.; Fettinger, J.; Eichhorn, B. *J. Am. Chem. Soc.* **2006**, *128*, 9178–9186.
(16) Esenturk, E. N.; Fettinger, J.; Lam, Y. F.; Eichhorn, B. *Angew. Chem., Int. Ed.* **2004**, *43*, 2132–2134.
(17) Cui, L. F.; Huang, X.; Wang, L. M.; Zubarev, D. Y.; Boldyrev, A. I.; Li, J.; Wang, L. S. *J. Am. Chem. Soc.* **2006**, *128*, 8390–8391.
(18) Cui, L. F.; Huang, X.; Wang, L. M.; Li, J.; Wang, L. S. *J. Phys. Chem. A* **2006**, *110*, 10169–10172.
(19) Spiekermann, A.; Hoffinann, S. D.; Fassler, T. F. *Angew. Chem., Int. Ed.* **2006**, *45*, 3459–3462.
(20) Esenturk, E. N.; Fettinger, J.; Eichhorn, B. *Chem. Commun.* **2005**, 247–249.
(21) Esenturk, E. N.; Fettinger, J.; Eichhorn, B. *Polyhedron* **2006**, *25*, 521–529.
(22) Goidoechea, J. M.; Sevov, S. C. *J. Am. Chem. Soc.* **2005**, *127*, 7676–7677.
(23) Goicoechea, J. M.; Sevov, S. C. *Angew. Chem., Int. Ed.* **2005**, *44*, 4026–4028.
(24) Goicoechea, J. M.; Sevov, S. C. *Organometallics* **2006**, *25*, 4530–4536.
(25) Goicoechea, J. M.; Sevov, S. C. *J. Am. Chem. Soc.* **2006**, *128*, 4155–4161.

10.1021/ic701699d CCC: $40.75
Published on Web 04/02/2008

Although the $M@Pb_{10}^{2-}$ and $M@Pb_{12}^{2-}$ ions have been observed in the gas phase for M = Ni, Pd, Pt,[7,15,16,20] the relative populations observed in the MS studies and solution NMR studies showed that Ni favors the 10-atom cluster (see I), whereas Pd and Pt favor the centered 12-atom icosahedron (see II).[15] This cluster preference can be understood in terms of steric effects and coordination preferences of the centered metals, where Ni prefers the smaller 10-atom cage and Pt and Pd prefer the larger icosahedral cavity.

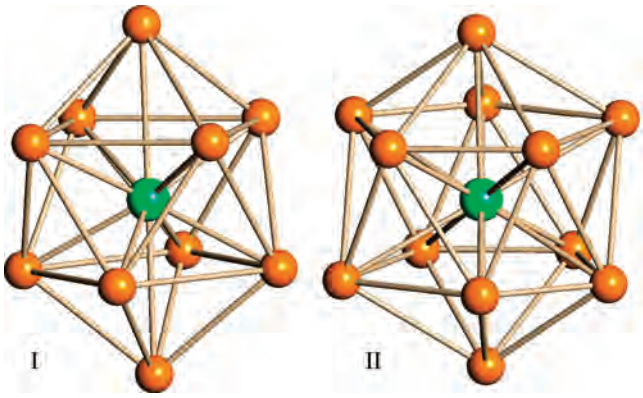

Not surprisingly, the chemistry of Sn_9^{4-} is intermediate to Ge_9^{4-} and Pb_9^{4-}. Like Pb_9^{4-}, Sn_9^{4-} readily fragments in reactions with transition metals to give disproportionated products such as $Sn_6[Nb(tol)]_2^{2-}$, $Ni_2@Sn_{17}^{4-}$, and $Pt_2@Sn_{17}^{4-}$.[8,10,26] However, most of the crystallographically characterized polystannides have structures reminiscent of the polygermanides, which are quite different from the $M@Pb_{10}^{2-}$ and $M@Pb_{12}^{2-}$ ions described above. While the clusters themselves are discrete, robust entities, most are highly dynamic in solution, showing rapid intramolecular exchange. For example, all 17 Sn atoms of $Pt_2@Sn_{17}^{4-}$ are in fast exchange on the NMR time scale at −50 °C, indicative of a liquid-like shell of Sn atoms around a Pt_2 core.[10]

In our continuing quest to understand the structural principles guiding the chemistry, dynamics, and stabilities of this class of compounds, we report here on the synthesis and properties of the unusual $Pd_2@Sn_{18}^{4-}$ anion. Surprisingly, the cluster has a nuclearity different from that of the Ni and Pt analogues, $Ni_2@Sn_{17}^{4-}$ and $Pt_2@Sn_{17}^{4-}$, and is isostructural with the germanium analogue, $Pd_2@Ge_{18}^{4-}$.[23] The solution dynamics and gas-phase chemistry also show interesting differences in comparison with those of $Pt_2@Sn_{17}^{4-}$, including its propensity to preferentially fragment to $Pd@Sn_{10}^{-}$ in the gas phase. Immediately prior to the submission of this paper, Sun et al. reported[27] a slightly different polymorph of the same anion. However, the gas-phase chemistry and the solution dynamics are reported here for the first time.

Results

Synthesis. Ethylenediamine (en) solutions of K_4Sn_9 react with toluene solutions of $Pd(PPh_3)_4$ in the presence of 2,2,2-cryptand to give low yields (∼15%) of $[K(2,2,2\text{-crypt})]_4[Pd_2@Sn_{18}]\cdot 3en$ as dark red-brown crystals. The salt is soluble in dmf and en but slowly decomposed in the former. The complex is air- and moisture-sensitive in solution and the solid state and has been characterized by EDX analysis, single-crystal X-ray diffraction, ^{119}Sn NMR spectroscopy, and LDI mass spectrometry.

The reaction between Sn_9^{4-} and $Pd(PPh_3)_4$ to give the title anion requires a net four-electron oxidation of the precursors. We[28] and others[29] have shown in previous studies that the oxidation occurs by way of reducing solvent molecules and, in some cases, reductive coupling of hydrocarbyl fragments of ancillary ligands. While not explicitly studied here, we assume that the same mechanisms are operative.

Table 1. Crystallographic Data for $[K(2,2,2\text{-crypt})]_4[Pd_2Sn_{18}]\cdot 3en$

empirical formula	$Pd_2Sn_{18}\cdot 4(C_{18}H_{36}N_2O_6)\cdot 3(C_2H_8N_2)$
formula wt	4191.88
temp	200(2) K
wavelength	0.71073 Å
cryst syst	triclinic
space group	$P\bar{1}$
unit cell dimens	
a	14.7979(9)
b	15.8742(10)
c	15.9343(10)
α	115.2830(10)
β	98.2450(10)
γ	100.8710(10)
V	3216.3(3) Å^3
Z	1
density, ρ_{calcd}	2.164 g/cm^3
abs coeff, μ	3.885 mm^{-1}
no. of data/restraints/params	11 311/216/669
goodness of fit on F^2	0.995
final *R* indices	
R1 ($I > 2\sigma(I)$)[a]	0.0476
wR2 (all data)[a]	0.0955

[a] $R1 = \sum||F_o| - |F_c||/\sum F_o$, $wR2 = [\sum w(F_o^2 - F_c^2)^2/\sum w(F_o^2)^2]^{1/2}$.

Table 2. Selected Bond Lengths (Å) for the $Pd_2@Sn_{18}^{4-}$ Ion

Pd1−Sn5	2.848(10)	Pd1−Sn1	2.865(11)	Pd1−Sn8	2.868(10)
Pd1−Sn2	2.876(11)	Pd1−Sn6	2.883(11)	Pd1−Sn3	2.878(10)
Pd1−Sn4	2.882(11)	Pd1−Sn9	2.882(10)	Pd1−Sn7	2.883(11)
Sn1−Sn2	3.003(11)	Sn1−Sn3	3.029(11)	Sn1−Sn9	3.048(10)
Sn1−Sn5	3.061(11)	Sn1−Sn4	3.251(11)	Sn2−Sn3	3.006(11)
Sn2−Sn5	3.048(11)	Sn2−Sn7	3.065(10)	Sn2−Sn6	3.274(11)
Sn3−Sn7	3.051(11)	Sn3−Sn9	3.056(11)	Sn3−Sn8	3.246(10)
Sn4−Sn9	3.040(10)	Sn4−Sn5	3.146(10)	Sn5−Sn6	3.089(11)
Sn6−Sn7	3.054(11)	Sn7−Sn8	3.065(10)	Sn8−Sn9	3.096(10)
Sn9−Sn6	3.079(11)				

Solid-State Structure. The $[K(2,2,2crypt)]_4[Pd_2@Sn_{18}]\cdot 3en$ salt crystallizes in the triclinic space group $P\bar{1}$, in which the $Pd_2@Sn_{18}^{4-}$ ion resides on the inversion center. A summary of the crystallographic data is given in Table 1, and bond distances and angles are given in Table 2.

The Sun report[27] described a slightly different polymorph with slightly different lattice parameters, but the anions are virtually identical. The $Pd_2@Sn_{18}^{4-}$ cluster has a capsulelike structure defined by a *closo*-Sn_{18} deltahedron with 2 endohedral Pd atoms (Figure 1). The complex has virtual D_{3d} point symmetry that gives rise to 3 chemically inequivalent sets of Sn atoms in a 6:6:6 ratio. The polyhedron has 48 edges

(26) Kesanli, B.; Eichhorn, B. W.; Fettinger, J. C. *Angew. Chem., Int. Ed.* **2001**, *40*, 2300–2302.
(27) Sun, Z.-M.; Xiao, H.; Li, J.; Wang, L.-S. *J. Am. Chem. Soc.* **2007**, *129*, 9560–9561.
(28) Kesanli, B.; Fettinger, J.; Gardner, D. R.; Eichhorn, B. *J. Am. Chem. Soc.* **2002**, *124*, 4779–4786.
(29) Ugrinov, A.; Sevov, S. C. *J. Am. Chem. Soc.* **2002**, *124*, 2442–2443.

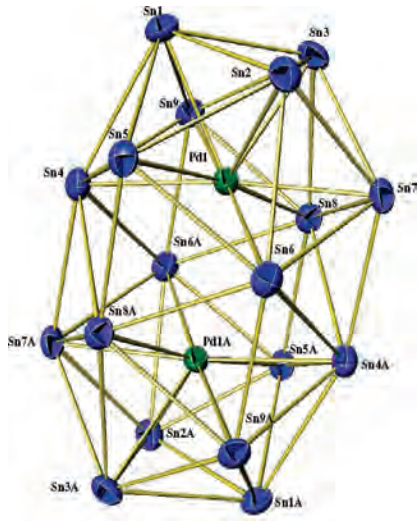

Figure 1. Crystal structure of the $Pd_2@Sn_{18}^{4-}$ cluster. Thermal ellipsoids are drawn at the 50% probability level.

and 32 triangular faces defined by 6 6-coordinate Sn atoms around the waist of the cluster and 12 5-coordinate Sn atoms at the ends of the cluster. The complex is isostructural with the germanium analogue[22] $Pd_2@Ge_{18}^{4-}$ and represents the largest polystannide characterized to date. The cage is also reminiscent of the $Cd_{18-x}Sn_x$ subunit found in $Na_{49}Cd_{58.5}Sn_{37.5}$.[30] The structure is quite similar to that of $Pt_2@Sn_{17}^{4-}$, except that the planar 6-membered ring at the center of $Pd_2@Sn_{18}^{4-}$ is replaced by a disordered 5-membered ring in the Pt complex.[10] The centered metal atoms are 9-coordinate in each of the clusters. In addition to having one fewer Sn atom, the M−M separation is much longer in $Pt_2@Sn_{17}^{4-}$ (D_{Pt-Pt} = 4.194(2) Å)[10] than in $Pd_2@Sn_{18}^{4-}$ (D_{Pd-Pd} = 3.384(15) Å). The Pd−Sn distances are in the range 2.849(10)–2.883(11) Å (average 2.87 Å), which is somewhat larger than the average Pt−Sn contacts (2.78 Å). The Sn−Sn contacts for $Pd_2@Sn_{18}^{4-}$ are in the range 3.003(11)–3.393(11) Å with an average of 3.11 ± 0.10 Å. While the Sn−Sn contacts in $Pt_2@Sn_{17}^{4-}$ span a larger range (2.867(2)–3.504(3) Å)[10] with a somewhat larger average (3.19 ± 0.19 Å), it has five Sn−Sn contacts under 3.0 Å. In comparison, only the Pd complex has no Sn−Sn contacts under 3.0 Å. At present, it is unclear to us why the Pd cluster has a different structure with longer M−Sn contacts relative to those of Pt.

NMR Spectroscopic Studies. Crystals of the K(2,2,2-crypts)$^+$ salt of the $Pd_2@Sn_{18}^{4-}$ ion dissolved in dmf show a single resonance in the ^{119}Sn NMR spectrum at temperatures between −50 and +10 °C (see Figure 2). The chemical shift is temperature dependent and moves from −733.8 ppm at −50 °C to −720 ppm at +10 °C. Above −10 °C, the cluster slowly reacts with the dmf solvent and decomposes. However, it is stable for weeks in en solvents, where it shows a room-temperature signal at −751.3 ppm. The variable-temperature ^{119}Sn spectra were measured at both 186.4 and 223.8 MHz using crystals dissolved at −50 °C that were immediately transferred to the spectrometer at −50 °C. On

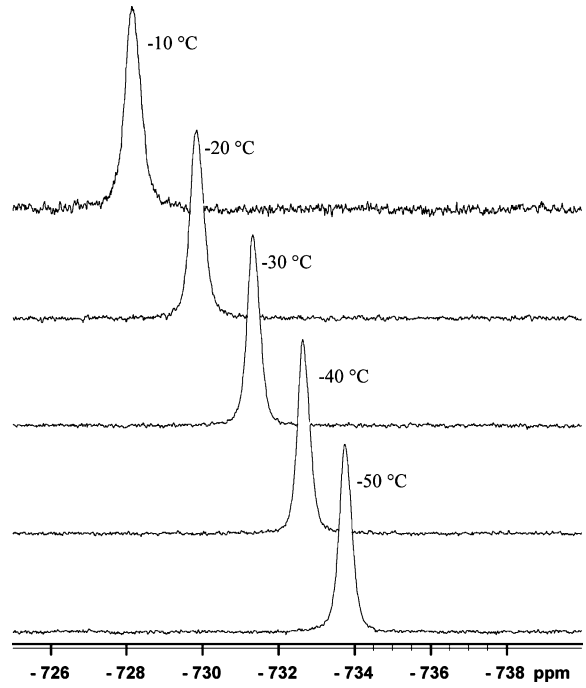

Figure 2. Temperature-dependent ^{119}Sn NMR spectra for $Pd_2@Sn_{18}^{4-}$ recorded from dmf solutions at 186.4 MHz and temperatures from –50 to –10 °C.

the basis of the solid-state structure, the limiting ^{119}Sn NMR spectrum is expected to have three mutually coupled, equal-intensity resonances, which is in contrast to the observed single resonance. The absence of additional peaks in the −2500 to +2500 ppm window, the lack of Sn−Sn coupling greater than 120 Hz (see below), and the similarities to the $Pt_2@Sn_{17}^{4-}$ spectrum[10] indicate that all 18 Sn atoms of the $Pd_2@Sn_{18}^{4-}$ cluster are in fast exchange on the ^{119}Sn NMR time scale at −50 °C.

The −734.0 ppm chemical shift is very similar to the −742.3 ppm resonance of $Pt_2@Sn_{17}^{4-}$. However, the Pt cluster shows $J_{117_{Sn}-119_{Sn}}$ = 170 Hz and $J_{195_{Pt}-119_{Sn}}$ = 774 Hz couplings[10] with intensities indicating coupling between two equivalent Pt atoms and 17 equivalent Sn atoms. These data unequivocally showed that all 17 Sn atoms and both Pt atoms are in fast exchange on the NMR time scale in the $Pt_2@Sn_{17}^{4-}$ ion from −50 °C to room temperature. The similarities in structures, composition, ^{119}Sn chemical shifts, and temperature dependencies between $Pt_2@Sn_{17}^{4-}$ and $Pd_2@Sn_{18}^{4-}$ suggest that the same rapid exchange is operative in the present Pd complex. However, the $J_{117_{Sn}-119_{Sn}}$ coupling observed for the Pt complex in not observed in the $Pd_2@Sn_{18}^{4-}$ ^{119}Sn NMR spectrum. From an evaluation of the line width of the resonance at −50 °C (see the Supporting Information), we know that the ^{119}Sn−^{117}Sn coupling constant in $Pd_2@Sn_{18}^{4-}$ is less than 120 Hz, which is surprising, in light of the similarity of structure and dynamics between the two clusters. If one assumes that the local $J_{117_{Sn}-119_{Sn}}$ values are the same between the two clusters, then only a slight 6% reduction in coupling would be anticipated on the basis of statistical averaging (i.e., 17/18) as has been observed in related systems.[10,28] The significant decrease in coupling suggests that the local $J_{117_{Sn}-119_{Sn}}$ values are substantially

(30) Todorov, I.; Sevov, S. C. *J. Am. Chem. Soc.* **1997**, *119*, 2869–2876.
(31) Wells, A. F.; *Structural Inorganic Chemistry*; 5th ed.; Oxford University Press: New York, 1991.

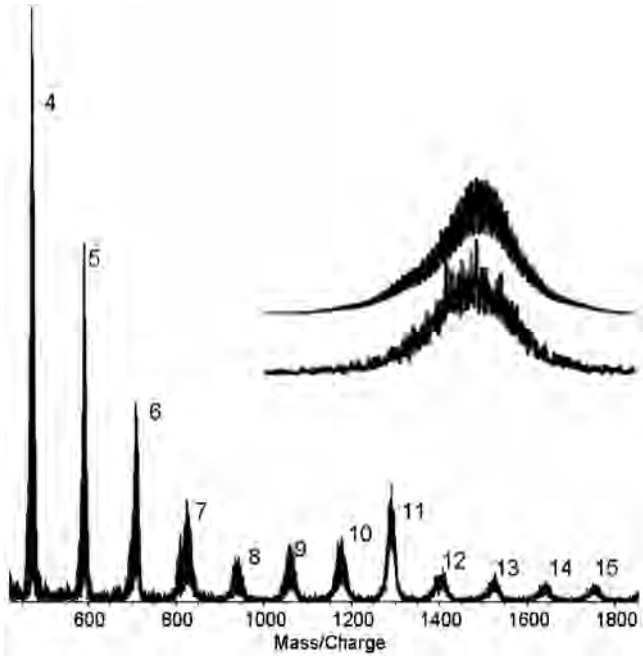

Figure 3. Negative ion LDI mass spectrum of $[K(2,2,2\text{-crypt})]_4[Pd_2Sn_{18}]\cdot 3en$ recorded from a crystalline sample deposited on carbon tape. The peak numbers correspond to "x" in the Sn_x^-, $PdSn_{x-1}^-$, $Pd_2Sn_{x-2}^-$, $Pd_3Sn_{x-3}^-$ series. The inset shows the simulated (top) and observed (bottom) mass envelope for the $x = 11$ region containing the $PdSn_{10}^-$ ion. See Table 3 for peak assignments and the Supporting Information for detailed simulation data.

lower on average in the $Pd_2@Sn_{18}^{4-}$ cluster. Alternatively, the exchange process could be intermolecular, which would eliminate $J_{117_{Sn}-119_{Sn}}$ coupling. While this scenario is possible, we believe that the exchange is intramolecular but with a mechanism of exchange that gives small average coupling constants. Such an intramolecular exchange has been documented[28] for $[Sn_9Pt_2(PPh_3)]^{2-}$.

The average Sn−Sn contacts of the two clusters are very similar; the $Pt_2@Sn_{17}^{4-}$ complex has more short Sn−Sn contacts[10] under 3.0 Å than does the $Pd_2@Sn_{18}^{4-}$ cluster. These short interactions presumably give rise to large, local $J_{117_{Sn}-119_{Sn}}$ values and may account for the larger Sn−Sn coupling in the Pt cluster. Alternatively, the intermediate structures in the exchange process may be very different in the two mechanisms and could give rise to the differences in Sn−Sn coupling.

Mass Spectrometry. A representative negative ion LDI mass spectrum of the $Pd_2@Sn_{18}^{4-}$ ion is shown in Figure 3. Data were collected from multiple samples that were prepared from either single crystals deposited directly onto carbon tape or from evaporated dmf solutions of crystalline samples. The latter gave the highest quality data and are presented here. The spectrum shows extensive fragmentation of the cluster, which is common for LDI MS studies for clusters of this type. Monoanions are exclusively observed in the MS spectra, which is also common in these situations.[28] Only a weak molecular ion peak is observed at 2345 amu, whereas several series of smaller cluster species dominate the gas-phase populations. Because the average isotopic masses of Pd and Sn are similar (Pd, 106.4 amu; Sn, 118.7 amu), overlapping series of Pd−Sn clusters are observed. At low mass, the palladium-free Sn_x^- series where $x = 1$–12 dominates the spectrum and contains previously described ions such as the D_{4d} Sn_{10}^- and I_h Sn_{12}^- clusters.[17] At higher masses, the $PdSn_{x-1}$, $Pd_2Sn_{x-2}^-$, $Pd_3Sn_{x-3}^-$, and $Pd_4Sn_{x-4}^-$ clusters grow in relative abundance and give rise to composite mass envelopes. Deconvolution of the mass envelopes through simulation provides reasonable estimates of the constituent cluster species. These data are summarized in Table 3 and shown graphically in the Supporting Information. Clusters larger than $x = 21$ were not observed.

Table 3. Relative Gas-Phase Populations[a] of Sn_x^-, $PdSn_{x-1}^-$, $Pd_2Sn_{x-2}^-$, $Pd_3Sn_{x-3}^-$, and $Pd_4Sn_{x-4}^-$

	population, %				
x	Sn_x	$PdSn_{x-1}$	Pd_2Sn_{x-2}	Pd_3Sn_{x-3}	Pd_4Sn_{x-4}
4	88	12			
5	87	13			
6	86	13	1		
7	76	20	4		
8	38	46	12	4	
9	36	44	16	4	
10	27	44	22	7	
11	6	64	27	3	
12	5	34	37	24	
13		39	32	21	8
14		32	39	21	8
15		15	42	34	9

[a] Relative percentages were estimated by fitting the mass envelopes using the KOMPACT simulation package. Calculated and observed spectra are shown in the Supporting Information.

The four Pd−Sn cluster series show Gaussian-like population distributions with increasing values of x (see Table 3). The major exception is the $PdSn_{10}^-$ ion, which shows an anomalously high abundance in the $PdSn_{x-1}^-$ series (see Figure 3 and Table 3). This cluster is most likely the oxidized product of $Pd@Sn_{10}^{2-}$ that presumably has the D_{4d} structure observed for the isoelectronic $Ni@Pb_{10}^{2-}$ ion.[20] Surprisingly, the $PdSn_{12}^-$ peak (the oxidized product of $Pd@Sn_{12}^{2-}$) shows only a small spike in abundance relative to the other $PdSn_x^-$ ions and appears to be significantly less stable than the $PdSn_{10}^-$ cluster. This phenomenon is similar to the product distribution observed for the $Ni@Pb_{12}^{2-}/Ni@Pb_{10}^{2-}$ series, where the latter was formed preferentially.[15] Moreover, the lack of a prominent molecular ion in the LDI spectrum is in contrast with the LDI MS measurements in many of our other systems[15,20,32] and suggests that the $Pd_2@Sn_{18}^{4-}$ ion may be a kinetic intermediate on the way to the $Pd@Sn_{10}^{2-}$ ion. The structures of the remaining clusters will require theoretical evaluation, but their presence clearly illustrates the diversity and richness of this bimetallic system.

Discussion

Reactions of Sn_9^{4-} with zerovalent group 10 metal complexes gives three different products: $Ni_2@Sn_{17}^{4-}$, $Pd_2@Sn_{18}^{4-}$, and $Pt_2@Sn_{17}^{4-}$.[8,10] Only the $Pd_2@Sn_{18}^{4-}$ cluster maintains the stoichiometry of the 9-atom Sn_9^{4-} precursor, whereas the other systems require fragmentation of the precursor and give two different 17-atom deltahedral structures. ^{119}Sn NMR studies of the respective reaction

(32) Moses, M. J.; Fettinger, J.; Eichhorn, B. *Science* **2003**, *300*, 778.

mixtures suggest that the isolated products are the predominant species in all three reactions. While all three clusters have some common features, such as Sn_6 capped pentagonal prisms and 9-coordinate transition metals, their individual structures are quite different. $Ni_2@Sn_{17}^{4-}$ contains two distinct $Ni@Sn_9$ clusters that share one common vertex (see III),[8] whereas $Pt_2@Sn_{17}^{4-}$ has a prolate, capsule-like structure in which the two Pt atoms occupy a common endohedral cavity (see IV).[10] The $Pd_2@Sn_{18}^{4-}$ structure is not intermediate to the Ni and Pt as we anticipated but takes on a structure of higher nuclearity and has a larger endoheral cavity than Pt. This variation in structure is in sharp contrast with that of the analogous Pb_9^{4-} chemistry, where Ni, Pd, and Pt all form $M@Pb_{10}^{2-}$ and $M@Pb_{12}^{2-}$ clusters. It is also surprising that Pd would template a larger Sn cluster than Pt in view of the smaller metallic radius of Pd (1.37 Å) versus that of Pt (1.39 Å).[31] The diversity in structures in the tin system and their differences from the corresponding lead clusters suggests that Sn_{10}^{2-} and Sn_{12}^{2-} clusters are less stabilizing hosts relative to the observed Sn_{17}^{4-} and Sn_{18}^{4-} cages and the corresponding Pb_{10}^{2-} and Pb_{12}^{2-} congeners. The MS data reported here and elsewhere[7] clearly show that the $M@Sn_{10}^{2-}$ and $M@Sn_{12}^{2-}$ clusters can be generated in the gas phase but are apparently less stable in solution. It is possible that the appropriate experimental conditions have not been achieved and the isolated clusters may represent kinetic products. Further experiments are in progress.

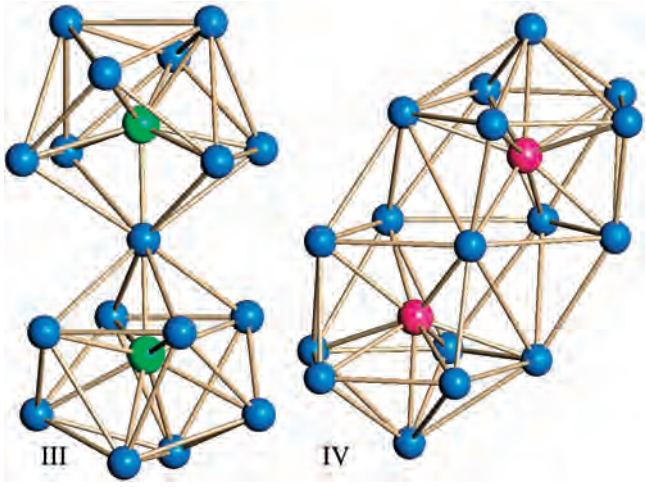

Finally, the NMR studies show that $Pd_2@Sn_{18}^{4-}$ and $Pt_2@Sn_{17}^{4-}$ are very dynamic in solution with rapid exchange of all Sn atoms at −50 °C. The $Ni_2@Sn_{17}^{4-}$ cluster is also dynamic, but the exchange can be slowed on the NMR time scale at low temperatures. The unusual feature of the $Pd_2@Sn_{18}^{4-}$ NMR signal is the small $J_{117_{Sn}-119_{Sn}}$ coupling constant, which is significantly less than that observed in the $Pt_2@Sn_{17}^{4-}$ cluster.[10] We believe that the smaller coupling may reflect the longer average Sn−Sn bond distances in the Sn_{18} cage of the former or a different exchange mechanism. To our knowledge, the $Pd_2@Sn_{18}^{4-}$ ion is the largest cluster to show fast global exchange on the NMR time scale.

Experimental Section

General Data. All reactions were performed in a nitrogen atmosphere drybox. The ^{119}Sn NMR spectra were recorded on a Bruker DRX500 Avance and AVANCE III 600 spectrometers operating at 186.4 and 223.8 MHz, respectively. In all measurements, to avoid RF heating, a high nitrogen flow rate was used in combination with the temperature controller. The pulse sequence used was the standard Bruker "zgdc" program and the standard Bruker "zgig" program for experiments done on DRX500 Avance and AVANCE III 600 spectrometers, respectively. A 30° pulse strength and 0.5 s relaxation delays were used. A macro automation program was written so that multiple block searches of 300 ppm were used in locating the ^{119}Sn signal. The spectral window −2500 to +2500 ppm was searched by this method. The signals were confirmed and verified by repeating the final measurements with different transmitter offsets. ^{119}Sn chemical shifts were referenced to Me_4Sn in C_6D_6 (0 ppm) at room temperature. The LDI-TOF MS studies were performed on a Kompact Maldi Axima-CFR spectrometer using a 337 nm nitrogen laser source with a 3 ns pulse width. The samples were mounted on carbon tape by depositing pure crystalline samples or by dissolving crystals in dmf, depositing the solutions onto the carbon tape, and drying. The sample plate was loaded into the spectrometer through an Ar-purged glovebag affixed to the sample chamber.

Chemicals. Melts of nominal composition K_4Sn_9 were made by fusion of stoichiometric ratios of the elements at high temperature. The chemicals were sealed in evacuated silica tubes and heated carefully with a natural gas/oxygen flame. ***Caution!*** Molten alloy synthesis can result in serious explosions, and reactions should be conducted with great caution behind blast shields. 4,7,13,16,21,24-Hexaoxa-1,10-diazobicyclo[8,8,8]hexacosane (2,2,2-crypt) was purchased from Aldrich. $Pd(PPh_3)_4$ was purchased from Sigma-Aldrich. Anhydrous ethylenediamine (en) and dimethylformamide (DMF) were purchased from Fisher, vacuum-distilled from K_4Sn_9, and stored under dinitrogen. Toluene was distilled from sodium/benzophenone under dinitrogen and stored under dinitrogen.

Synthesis of $[K(2,2,2\text{-crypt})]_4[Pd_2@Sn_{18}]$. In vial 1, K_4Sn_9 (80 mg, 0.065 mmol) and 2,2,2-crypt (98 mg, 0.26 mmol) were dissolved in en (∼2 mL) and stirred for ∼5 min, yielding a red-brown solution. In vial 2, $Pd(PPh_3)_4$ (75 mg, 0.065 mmol) was dissolved in tol (∼1 mL) yielding a pale yellow solution. The solution from vial 2 was added dropwise to vial 1, and the mixture was stirred for about 2 days, yielding a reddish brown solution. The solution was then filtered through tightly packed glass wool. After 5 days, ∼25 mg of reddish black crystals of $[K(2,2,2\text{-crypt})]_4[Pd_2@Sn_{18}]$ were obtained. Yield: ∼15%.

Crystallography. A dark brown prism of $(C_{18}H_{36}N_2O_6K)_4[Pd_2Sn_{18}]\cdot 3(C_2H_8N_2)$, approximate dimensions 0.015 × 0.04 × 0.250 mm^3, was used for the X-ray crystallographic analysis. The X-ray intensity data were measured at 200(2) K on a three-circle diffractometer system equipped with a Bruker Smart Apex II CCD area detector using a graphite monochromator and a Mo Kα fine-focus sealed tube (λ = 0.710 73 Å) operated at 50 kV and 40 mA. The detector was placed at a distance of 5.500 cm from the crystal.

A total of 1830 frames were collected with a scan width of 0.3° in ω and an exposure time of 30 s/frame. The total data collection time was 18.1 h. The frames were integrated with the Apex2 software package using a narrow-frame integration algorithm. Data were corrected for absorption effects using SADABS. The minimum and maximum transmission coefficients were 0.750 and 0.943.

The structure was solved and refined using the SHELXS-97 using standard operation procedures described in our laboratory. The

hydrogen atoms on the crypt group and the disordered en solvate were restrained in the final cycles. The largest peak on the final difference map was 1.520 e/Å^3, and the largest hole was −1.121 e/Å^3.

Acknowledgment. This material is based upon work supported by the National Science Foundation under Grant No. 0401850.

Supporting Information Available: A CIF file, giving crystal data for $Pd_2@Sn_{18}^{4-}$ and figures giving additional NMR and LDI-MS data and simulations. This material is available free of charge via the Internet at http://pubs.acs.org.

IC701699D